

# Numerical solutions for the surface diffusion flow in three space dimensions

Uwe F. Mayer

## Abstract

The surface diffusion flow is a moving boundary problem that has a gradient flow structure, and this gradient flow structure suggests an implicit finite-differences approach to compute numerical solutions. The resulting numerical scheme allows to compute the flow for any smooth orientable immersed initial surface. We provide an analytical proof of this gradient structure, and construct a discretization of the Laplacian of a scalar function on a triangulated surface. Then we describe the resulting numerical scheme, and conclude with several numerical experiments.

**Key words.** Numerical simulation, surface diffusion, mean curvature, Laplacian, gradient flow, free boundary problem, immersed surface.

**AMS subject classification 2000.** 35R35, 65M99.

## 1 Introduction

In this paper we study numerically the motion of a family of immersed surfaces whose normal velocity is equal to its surface diffusion. More precisely, let  $\Gamma_0$  be a smooth compact closed immersed orientable surface in  $\mathbb{R}^3$  of class  $C^{2+\beta}$ . It has been shown by Escher, Simonett, and the author in [15, 16] that then there exists a family  $\{\Gamma(t) : 0 \leq t < T\}$  of smooth immersed orientable surfaces satisfying the following evolution equation:

$$V = \Delta\kappa, \quad \Gamma(0) = \Gamma_0. \quad (1.1)$$

Here  $V$  denotes the velocity in the normal direction of  $\Gamma(t)$ , while  $\Delta$  and  $\kappa$  stand for the Laplace-Beltrami operator and the mean curvature of  $\Gamma(t)$ , respectively. Both the normal velocity and the curvature depend on the choice of the orientation, however, (1.1) does not, and so we are free to choose whichever one we like. In particular, if  $\Gamma(t)$  is embedded and encloses a region  $\Omega(t)$  we always choose the outer normal, so that  $V$  is positive if  $\Omega(t)$  grows, and so that  $\kappa$  is positive if  $\Gamma(t)$  is convex with respect to  $\Omega(t)$ . Due to the local nature of the evolution we may assume the surface  $\Gamma_0$  to be connected.

In a previous paper [24] the author has shown how to set up a numerical scheme for certain free boundary problems that are gradient flows for the area functional, the specific notion of gradient flow being due to P. Fife [17, 18]. This paper is an extension of the work therein. We will show that the surface diffusion flow coincides with the  $H_0^{-1}$  gradient flow of the area, a result that appears already in [9] (the presentation there has somewhat less detail with regard to the involved regularity questions), and which also is mentioned in [6, 10, 16, 29]. Then we will present the necessary steps to adapt the algorithm from [24] to compute numerical solutions. In particular we will develop a method to compute an approximation of the Laplacian of a function defined on a triangulated surface.

The proposed algorithm is a front-tracking boundary-integral method. It has the advantage that one does not have to differentiate across the front, as compared to a possible level-set approach. Also, because the  $H_0^{-1}$  inner product is described by an operator of local character (the Laplace-Beltrami operator on the interface), it makes no difference whether the moving interface is immersed or embedded. On the other hand, a level-set approach would be superior for investigation of topological changes or corner and cusp development, which lead to the breakdown of our numeric scheme. For two space dimensions a level-set approach to the surface diffusion flow can be found in [1], results for the surface diffusion flow using a level-set approach in three space dimensions are not known to the author. Both front-tracking methods and the level-set methods have been used intensively in the literature for free boundary problems, see for example the review article by Hou [22].

The scheme will be used to perform several numerical experiments. The observed phenomena are manifold. A dumbbell with a sufficiently thin neck will pinch off, thereby forming an essential singularity because the curvature becomes infinite. On the other hand, a dumbbell with a thick neck will overcome this initial inward tendency, and will evolve into a sphere. A surface shaped like an erythrocyte (a red blood cell) with a thin enough center will cease to be embedded and become immersed, similarly to the behavior of a dumbbell in two dimensions. For the two-dimensional case, this behavior was conjectured by Elliot and Garcke [14], numerically confirmed with the algorithm presented herein by Escher, Simonett, and the author [16], and analytically proven by Giga and Ito [20]. For arbitrary dimensions the same result holds, as numerically and analytically established by Simonett and the author [25]. This example is not presented herein, as it can be found in the work quoted above. A long cylinder (with suitable end-caps) loses its convexity before it becomes convex again, and ultimately becomes spherical. This duplicates a result previously numerically obtained by Coleman, Falk, and Moakher [11, 12]; they use cylindrical coordinates and work with radially symmetric evolutions only, as in contrast to the scheme herein, which does a priori not use any of the symmetries of the given surfaces, but can be modified to use rotational symmetry if present. An analytical proof of this loss of convexity is due to Giga and Ito [21]. Finally, to clearly exhibit the differences between the model in two and three space dimensions, respectively, we consider the evolution of a tubular neighborhood of a finite spiral, and of a figure eight. In two dimensions there are numerical examples of embedded spirals that become immersed, but ultimately contract to an (embedded) circle [15]. In three dimensions, however, a tubular neighborhood of a spiral can develop a pinch-off. A figure eight in two dimensions contracts to a point, in a

seemingly self-similar fashion (if there actually are self-similar solutions to the surface diffusion flow is an open problem). In three space dimensions, however, the tubular neighborhood of a figure eight develops again an essential singularity.

The motion given by equation (1.1) has some interesting geometrical features. Assume that  $\{\Gamma(t) : 0 \leq t < T\}$  is a smooth solution to (1.1) and let  $\mathcal{A}(t)$  denote the area of  $\Gamma(t)$ . Then the function  $\mathcal{A}$  is smooth and we find for its derivative (see e.g. [23, Theorem 4] or [19, p. 70])

$$\frac{d}{dt}\mathcal{A}(t) = \int_{\Gamma(t)} V \kappa \, d\sigma = \int_{\Gamma(t)} (\Delta \kappa) \kappa \, d\sigma = - \int_{\Gamma(t)} |\nabla \kappa|^2 \, d\sigma \leq 0,$$

where the gradient and absolute value are computed with respect to the metric of  $\Gamma(t)$ . Hence the motion driven by surface diffusion is area decreasing. Assume additionally that the solution consists of embedded surfaces which enclose a region  $\Omega(t)$ , and let  $\text{Vol}(t)$  denote the volume of  $\Omega(t)$ . The derivative of the smooth function  $\text{Vol}$  is then given by (assuming a compatible choice of orientation and sign of normal velocity)

$$\frac{d}{dt}\text{Vol}(t) = \int_{\Gamma(t)} V \, d\sigma = \int_{\Gamma(t)} \Delta \kappa \, d\sigma = 0, \tag{1.2}$$

thus the motion driven by surface diffusion is also volume preserving in the embedded case. In addition, every compact surface of constant mean curvature is an equilibrium for (1.1), as for example a Euclidean sphere or a Wente torus [30, 31].

The surface diffusion flow (1.1) was first proposed by Mullins [26] to model surface dynamics for phase interfaces when the evolution is only governed by mass diffusion in the interface. It has also been examined in a more general mathematical and physical context by Davì and Gurtin [13], and by Cahn and Taylor [9, 10]. More recently, Cahn, Elliott, and Novick-Cohen [8] showed by formal asymptotics that the surface diffusion flow is the singular limit of the zero level set of the solution to the Cahn-Hilliard equation with a concentration dependent mobility. In the related case of constant mobility in the Cahn-Hilliard equation, Alikakos, Bates, and Chen [3] proved that the motion of the singular limit is governed by the Mullins-Sekerka model (also called the Hele-Shaw model with surface tension), rigorously establishing a result that was formally derived by Pego [28].

In two dimensions and for strip-like domains only, the surface diffusion flow was investigated by Baras, Duchon, and Robert [5]. They prove global existence for rather weak assumptions on the initial data. Also in two dimensions, the surface diffusion flow for closed embedded curves was analytically investigated by Elliott and Garcke [14]. They show local existence and regularization for  $C^4$  initial curves, but have no uniqueness result, and they also show global existence for small perturbations of circles. Furthermore, assuming global existence, they prove that any embedded closed curve that stays embedded will become circular under this evolution. Polden [29] and, independently, Giga and Ito [20] show short-term existence and uniqueness for  $H^4$  initial curves. Finally, Escher, Simonett, and the author [15, 16] obtain short-term existence, smoothness, and uniqueness for immersed  $C^{2+\alpha}$  hypersurfaces in any space dimension, and also obtain global existence for small perturbations of spheres.

## 2 The gradient flow setup

We limit ourselves to the surface diffusion flow, for a more general introduction to gradient flows see [24], and in particular the notes by P. Fife [17, 18].

Gradient flows are a natural model for the dynamics of a system that is known to decrease some quantity  $\mathcal{A}$  as time evolves; that is, one seeks to solve

$$\frac{du(t)}{dt} = -\nabla\mathcal{A}(u(t)) \quad (2.1)$$

where  $u(t)$  describes the state of the system. In this paper the system will be characterized by a compact connected 2-dimensional surface  $\Gamma(t)$  immersed in  $\mathbb{R}^3$ , and  $\mathcal{A}$  will be the 2-dimensional surface area functional. (However, everything in this section works just as well in higher space dimensions. We actually never use that the setting is the 3-dimensional case.) In the formal equation (2.1) one should therefore think of  $u(t)$  as describing the position and shape of the interface  $\Gamma(t)$ , and we will see that  $du(t)/dt$  should be thought of as the normal velocity of  $\Gamma(t)$ . We know that the surface diffusion flow is smooth [15], that is, for small enough times  $\tau$  we have

$$\Gamma(t + \tau) = \{x \in \mathbb{R}^3 : x = y + \rho(y, t, \tau)N(y, t), y \in \Gamma(t)\}$$

for some smooth function  $\rho$  and chosen unit normal  $N$  of  $\Gamma(t)$ . Let  $V(y, t) = \frac{\partial\rho}{\partial\tau}(y, t, \tau)\Big|_{\tau=0}$  denote the normal velocity of  $\Gamma(t)$ . The following basic formula from differential geometry is our starting point:

$$\frac{d}{dt}\mathcal{A}(\Gamma(t)) = \int_{\Gamma(t)} V(x, t)\kappa(x, t) d\sigma_x, \quad (2.2)$$

where  $\kappa$  denotes mean curvature of  $\Gamma(t)$ . Throughout this paper the mean curvature is defined as the sum of the principal curvatures; this avoids having a factor of 2 in formula (2.2) above.

For the following we will need several spaces consisting of functions defined on the moving interface. For any fixed  $\Gamma = \Gamma(t)$  the space  $L_0^2(\Gamma)$  consist of all square-integrable functions with average zero, and the space  $H_0^1(\Gamma) \subset L_0^2(\Gamma)$  consists of those functions that additionally have square-integrable first-order weak derivatives. We write  $H_0^{-1}(\Gamma)$  for the dual space of  $H_0^1(\Gamma)$ , using the duality pairing inherited from  $L_0^2(\Gamma)$ . Finally,  $\mathbf{H}(\Gamma) := C_0^\infty(\Gamma) \subset H_0^{-1}(\Gamma)$  is the pre-Hilbert space we will be working with, the sub-index 0 again denoting that the average of the functions is zero. Note that the space  $\mathbf{H}(\Gamma)$  is endowed with the metric of  $H_0^{-1}(\Gamma)$ , which is the reason why we write  $\mathbf{H}(\Gamma)$  and not just  $C_0^\infty(\Gamma)$ .

The right-hand side of equation (2.2) can be interpreted as defining a linear functional for the function  $V$ ,

$$d\mathcal{A}/dt : \mathbf{H}(\Gamma) \rightarrow \mathbb{R}, \quad V \mapsto \int_{\Gamma} V \kappa d\sigma. \quad (2.3)$$

This linear functional is well-defined on  $\mathbf{H}(\Gamma)$ . We will show below that for the surface diffusion flow this functional is bounded for each surface  $\Gamma = \Gamma(t)$ . As  $\mathbf{H}(\Gamma)$  is dense in  $H_0^{-1}(\Gamma)$  we may extend the functional uniquely to the bigger space, and thus, by the Riesz representation

theorem, we can represent the functional as the scalar product with some unique element  $\nabla_{\mathbf{H}(\Gamma)}\mathcal{A} \in H_0^{-1}(\Gamma)$ , which we will show to be in  $\mathbf{H}(\Gamma)$  as well. Hence for any  $v \in \mathbf{H}(\Gamma)$

$$\int_{\Gamma} v \kappa d\sigma = \langle v, \nabla_{\mathbf{H}(\Gamma)}\mathcal{A} \rangle_{\mathbf{H}(\Gamma)}, \quad (2.4)$$

and in particular the following equation holds:

$$\frac{d\mathcal{A}}{dt} = \langle V, \nabla_{\mathbf{H}(\Gamma)}\mathcal{A} \rangle_{\mathbf{H}(\Gamma)}.$$

Finally,  $\Gamma(t)$  is said to be an  $\mathbf{H}$ -gradient flow for  $\mathcal{A}$  if for all times  $t$  the normal velocity satisfies

$$V(., t) = -\nabla_{\mathbf{H}(\Gamma(t))}\mathcal{A}. \quad (2.5)$$

Notice that the space with respect to which the gradient is computed is constantly changing.

The Laplace-Beltrami operator  $-\Delta$  on the surface  $\Gamma$  has a self-adjoint positive-definite realization on  $L_0^2(\Gamma)$ , and there is the following isometric isomorphism of function-spaces [4, Corollary 1.3.9, Theorem 1.4.12]

$$L_0^2(\Gamma) \rightarrow H_0^{-1}(\Gamma), \quad u \mapsto (-\Delta)^{1/2}u.$$

In particular for  $u, v \in \mathbf{H}(\Gamma)$  this implies [4, Theorem 1.5.15]

$$\langle u, v \rangle_{\mathbf{H}(\Gamma)} = \langle (-\Delta)^{-1/2}u, (-\Delta)^{-1/2}v \rangle_{L_0^2(\Gamma)} = \langle u, (-\Delta)^{-1}v \rangle_{L_0^2(\Gamma)}, \quad (2.6)$$

where we have used the self-adjointness of  $(-\Delta)^{-1/2}$  for the last equality. For ease of notation we set

$$S := (-\Delta)^{-1} : \mathbf{H}(\Gamma) \rightarrow \mathbf{H}(\Gamma),$$

and hence we can rewrite (2.6) as

$$\langle u, v \rangle_{\mathbf{H}(\Gamma)} = \langle u, Sv \rangle_{L_0^2(\Gamma)}.$$

For any  $V \in L_0^2(\Gamma)$  and  $\kappa \in C^\infty(\Gamma)$  we have, with  $\bar{\kappa}$  denoting the average of  $\kappa$ ,

$$\begin{aligned} \int_{\Gamma} V(x)\kappa(x) d\sigma_x &= \int_{\Gamma} V(x)(\kappa(x) - \bar{\kappa}) d\sigma_x \\ &= \langle V, \kappa - \bar{\kappa} \rangle_{L_0^2(\Gamma)} \\ &= \langle V, SS^{-1}(\kappa - \bar{\kappa}) \rangle_{L_0^2(\Gamma)} \\ &= \langle V, S^{-1}(\kappa - \bar{\kappa}) \rangle_{\mathbf{H}(\Gamma)}. \end{aligned}$$

This representation shows first of all that the functional from (2.3) is bounded if  $\kappa$  is smooth, and secondly, comparing this with (2.4) yields

$$\nabla_{\mathbf{H}(\Gamma)}\mathcal{A} = S^{-1}(\kappa - \bar{\kappa}),$$

so that in particular  $\nabla_{\mathbf{H}(\Gamma)}\mathcal{A} \in \mathbf{H}(\Gamma)$ . For the surface diffusion flow we know that  $\kappa$  is smooth, assuming the initial surface is smooth, which in turn follows from the proofs in [16]. This shows the claims made in the text following equation (2.3). Finally, equation (2.5) can be rewritten as

$$V(., t) = -S^{-1}(\kappa(., t) - \bar{\kappa}(t)). \quad (2.7)$$

Because of the definition of  $S$  it is obvious that equation (2.7) above is equivalent to definition (1.1) of the surface diffusion flow. In other words, the gradient flow for the area with respect to the  $H_0^{-1}$  metric coincides with the surface diffusion flow.

### 3 Discretization

This section uses heavily the setup from [24]. For the sake of brevity we only repeat here what is necessary. However, as we deal with the surface diffusion flow only, we will use  $\Delta$  in the sequel instead of the more general notation with the operator  $S$ .

#### 3.1 Discretization in time

For the gradient flow given through

$$V(x, t) = \Delta(\kappa(x, t) - \bar{\kappa}(t))$$

we pick a time step  $h > 0$ , and we use the implicit finite-difference equation

$$N(x, t) \cdot \frac{\Gamma(x, t+h) - \Gamma(x, t)}{h} = \Delta(\kappa(x, t+h) - \bar{\kappa}(t+h)).$$

Here  $\Gamma(x, t)$  stands for a parameterization of the surface  $\Gamma(t)$  over some fixed reference manifold, for example  $\Gamma_0$ . In the above equation one should actually write  $\tilde{\Gamma}$  and so on because it describes approximate solutions; by a similar abuse of notation we will call the left side of the above equation  $V(x, t)$  again and hence

$$\begin{aligned} \Gamma(x, t+h) &= \Gamma(x, t) + hV(x, t)N(x, t), \\ V(x, t) &= \Delta(\kappa(x, t+h) - \bar{\kappa}(t+h)). \end{aligned}$$

Finally we approximate the dependency of the curvature on the next time step by

$$\kappa(x, t+h) \approx \kappa(x, t) + hL(V(x, t))$$

where  $L$  is a linear operator which is formally defined via

$$L(V(x, t)) = \left. \frac{d}{dh} \kappa(\Gamma(x, t) + hV(x, t)N(x, t)) \right|_{h=0}. \quad (3.1)$$

As  $V(x, t)$  is in the range of  $\Delta$  it has average zero, and hence by linearity of  $L$  so does  $L(V(x, t))$ , thus

$$V(x, t) = \Delta(\kappa(x, t) + hL(V(x, t)) - \bar{\kappa}(t)).$$

This finally leads to the (semi-)implicit scheme given by

$$(I - h\Delta)LV(x, t) = \Delta(\kappa(x, t) - \bar{\kappa}(t)), \quad (3.2)$$

where  $I$  stands for the identity map.

### 3.2 Spatial discretization

For the spatial discretization triangulate the surface, and approximate any function defined on the surface by its values at the vertices of this triangulation. The Laplace-Beltrami operator  $\Delta$  on the surface  $\Gamma(t)$  is a linear operator on functions  $f$  defined on the surface, and hence we will approximate the value of  $\Delta f$  at a vertex  $z_k$  with

$$\Delta f(z_k) = - \sum_j s_{kj} f(z_j)$$

for a matrix  $(s_{kj})$  defined further below. (The minus sign is chosen to keep the notation compatible with [24].) Similarly let  $(l_{kj})$  be the matrix representing the linearization  $L$  of the curvature operator, for the details again see [24]. The numerical scheme is then given by the discretized version of (3.2),

$$\forall i : \quad \sum_j (\delta_{ij} + \sum_k h s_{ik} l_{kj}) V(z_j, t) = - \sum_j s_{ij} (\kappa(z_j, t) - \bar{\kappa}(t)). \quad (3.3)$$

Due to discretization effects the computed normal velocity will not have an average of exactly zero, in contrast to the analytical solution. One consequence of this, in the embedded case, would be a slight change of the enclosed volume as the flow progresses, compare equation (1.2). We will therefore, at each discrete time step, compute the average of the (discretized) normal velocity as computed with (3.3), and then subtract it. For a demonstration of the effect of this adjustment see section 4.1.

For a small disk  $D_\epsilon(z)$  centered at a point  $z$  on the surface, and a sufficiently smooth function  $f$  defined on the surface, Green's formula reads

$$\int_{D_\epsilon(z)} \Delta f(x) dx = \int_{\partial D_\epsilon(z)} \partial_\nu f(s) ds,$$

where  $\nu$  is the intrinsic outer normal of the boundary of the disk;  $\nu$  is tangential to the surface. For the triangulated surface replace the disk by the star of a vertex  $z_k$ , and approximate the average of  $\Delta f$  on the star by its value at the center vertex. For a vertex  $z_j$  on the boundary of  $\text{star}(z_k)$  approximate  $\partial_\nu f(z_j)$  by the finite difference quotient of  $f$  at  $z_j$  and  $z_k$ . To write down the approximation, let  $A_k$  be the area of  $\text{star}(z_k)$ , and for two consecutive vertices  $z_i$  and  $z_j$  on the boundary of the star of  $z_k$ , let  $d_{kj}$  be the distance between them. Then the approximation reads

$$\Delta f(z_k) = \frac{1}{A_k} \sum_{\text{star}(z_k)} \frac{d_{kj} + d_{k,j+1}}{2} \cdot \frac{f(z_j) - f(z_k)}{|z_j - z_k|} =: - \sum_j s_{kj} f(z_j).$$

Only coefficients  $s_{kj}$  with  $z_j$  in the star of  $z_k$  are nonzero. This reflects that the Laplace-Beltrami operator is a local operator. It can be used when one computes the products of this matrix in formula (3.3), keeping the number of floating-point operations quadratic instead of cubic in the number of vertices. This assumes one has a bound for the number of vertices in the star of a vertex, which is in fact less than 10 or so in all of the experiments below. The main computational work then consist of inverting the matrix on the left-hand side of (3.3), once for each time step. In our application  $f$  will of course be the mean curvature function  $\kappa$ .

### 3.3 Algorithms changing the triangulation

The spatial discretization used will most likely not remain to be a uniform triangular mesh on the surface, but vertices tend to accumulate at certain spots. This leads to difficulties in the scheme, where, at various steps, one has to divide by the distance between two vertices, and by the area of a facet. We propose the following three adaptive measures.

1. If an edge becomes too small, then one should combine the two vertices that make up this edge into their midpoint. In this process one has to be careful not to create vertices of valence two, such vertices need to be removed also. We call the relevant parameter the *minimal edge length*.

2. If an edge becomes too long, then one should subdivide the edge by adding a new vertex in the middle of the edge. This creates two new facets as well. The relevant parameter is called *maximal edge length*.

3. If a facet becomes too thin, then we propose to subdivide the base of the triangle by inserting a vertex at the base of the hight line, thereby creating two new facets. Here “thinness” is measured as the minimal hight of the triangle, the corresponding threshold parameter is called *minimal thinness* and should be less than the minimal edge length defined above. The newly created hight line of the thin triangle will then be removed according to step 1, and hence the thin facet has been removed.

These three strategies have been used in the experiments below. This is best seen in the example of the torus in section 4.3, where vertices need to be removed in the center, and others need to be added away from the inner loop.

## 4 Numerical experiments

The algorithm for the computations has been implemented using the programming language C, while the results of the computations were displayed using the Geomview package [27]. The surface graphs were transformed into a printable format with XV [7].

### 4.1 Two dumbbells

Rotation of a dumbbell curve about its long axis results in the usual dumbbell surface. (Rotation about the short axis creates a surface looking like a red blood cell. For numerical and analytical results concerning such surfaces see [25].) A dumbbell with a pinched-enough neck has its maximum of the mean curvature at the neck, and hence the Laplacian of the mean curvature

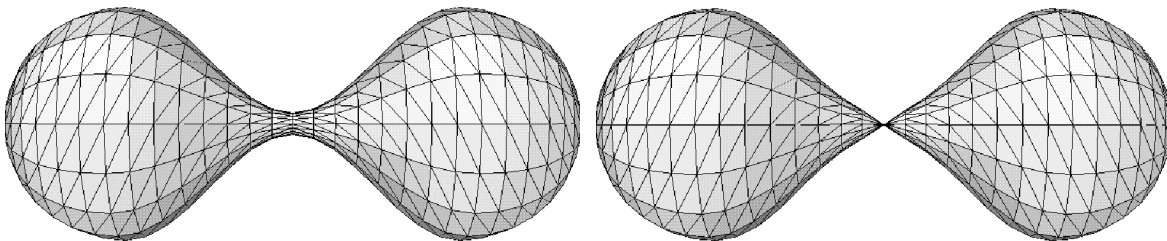


Fig. 1 A dumbbell with a sufficiently thin neck leads to a pinch-off. The first graph is the starting configuration, the second is at time  $t = 0.0044$ . The length of the dumbbell is about 11 units, the initial diameter at the neck is about 0.4 units.

will be negative. This leads to an inwards motion at the neck, and hence to an increased pinching effect, so that pinching-off can be expected, and in fact, it occurs. For this experiment (see Fig. 1) the maximal edge-length was set to 1, the minimal edge-length to 0.01, the minimal thinness of the facets to 0.005, and the time step to 0.0001. The surface has 498 vertices and 992 facets initially, and 485 vertices and 966 facets at the time of pinch-off. This computation is similar to one already presented in [15], and it is included here for the sake of completeness, and to show the contrast to the experiment below.

However, if the neck is too big, then relaxation will lead to (local) equalization of the surface tension and the neck will not pinch off. The dumbbell below is constructed of two spherical ends, the smaller one has radius 2.5, while the bigger one has radius 3. The radius of the neck is 1, the shape of the neck is obtained by rotating parts of suitably scaled sine functions. The evolution is similar to the effect that one would observe with the volume preserving (averaged) mean curvature flow, where the smaller sphere gets absorbed by the bigger one. (The mean curvature result was obtained with the algorithm from [24].) For this experiment (see Fig. 2) the maximal edge-length was set to 1.5, the minimal edge-length to 0.01, the minimal thinness of the facets to 0.005, and the time step to 0.01. The surface has 498 vertices and 992 facets initially. The last graph in Fig. 2 is almost spherical, the maximum and the minimum of the mean curvature differ by about 1.6 percent of the average of the mean curvature.

As this experiment displays the long-term behavior we will consider the enclosed volume, which can easily be computed as a surface integral using Green's formula. The enclosed volume is preserved by the exact solution, see (1.2). Due to the cumulative effects of discretization errors this is not exactly true for the numerical solution, but almost so. We then also perform the computations without forcing the average of the discretized normal velocity to be zero, as explained in section 3.2. The surface evolution is qualitatively not affected by this change of algorithm (i.e. the surfaces look the same), however quantitatively there is a difference, see Fig. 3. Hence the cumulative effect of computing the normal velocity directly with (3.3) should not be ignored, and subtracting the average of it at each step improves the accuracy of the

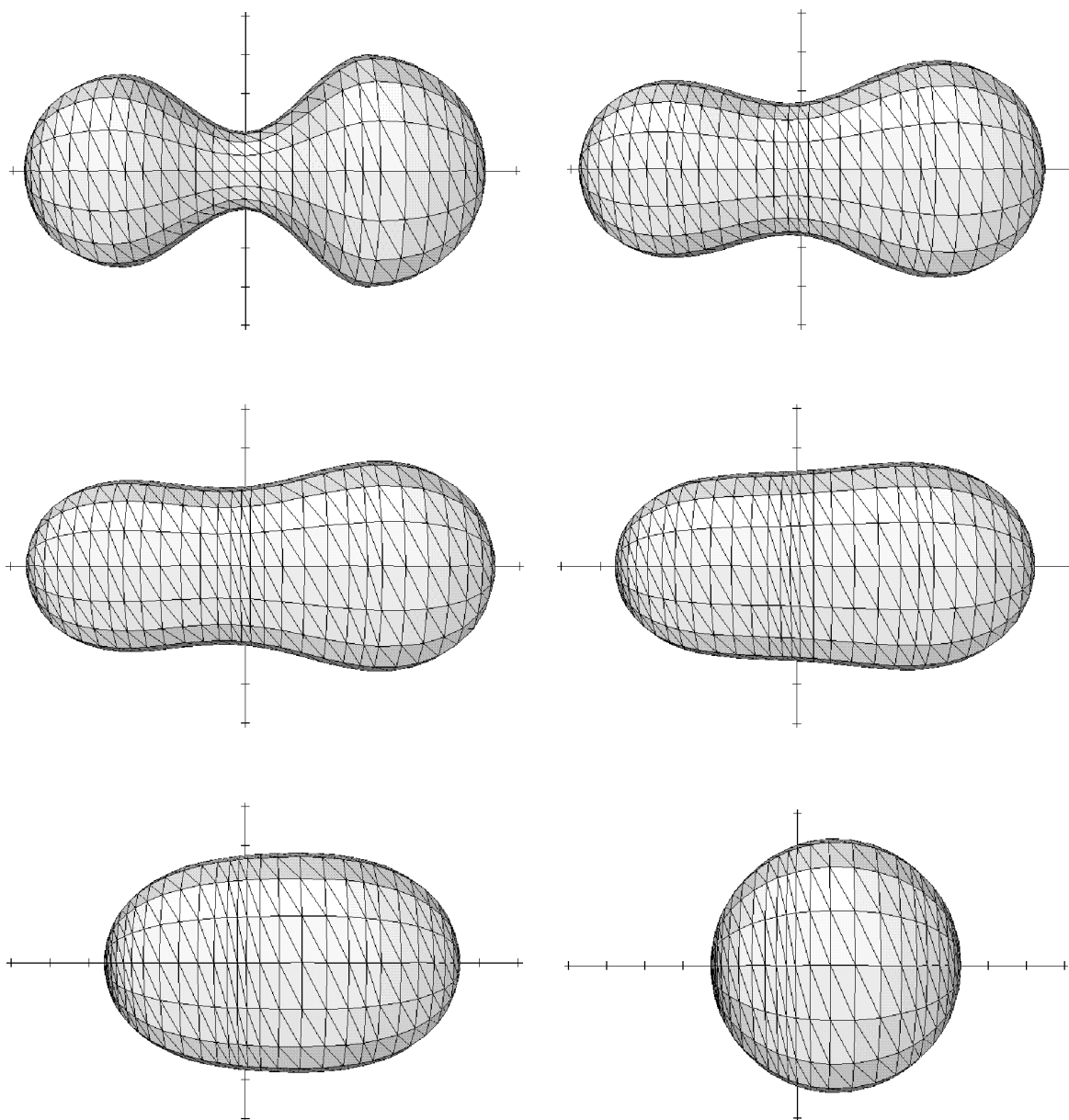


Fig. 2 A dumbbell with a sufficiently thick neck evolves into a sphere. The order of the graphs is top left ( $t = 0$ ), top right ( $t = 5$ ), middle left ( $t = 10$ ), middle right ( $t = 20$ ), bottom left ( $t = 30$ ), and bottom right ( $t = 80$ ). The length of the initial dumbbell is about 12 units.

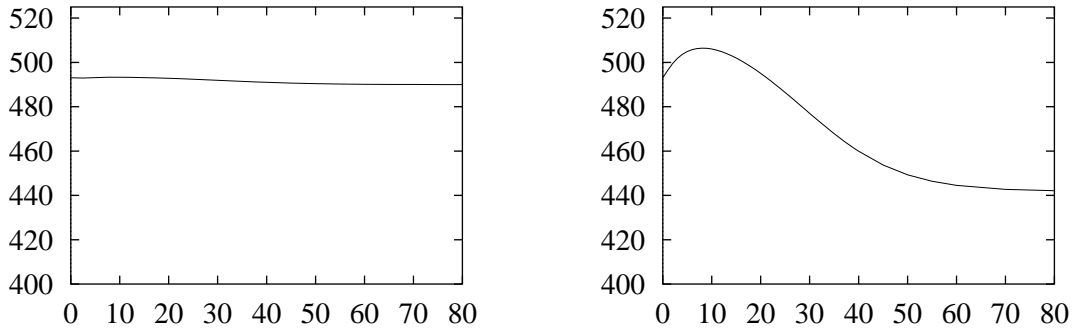


Fig. 3 This is a graph of the enclosed volume of the dumbbell with a thick neck as a function of time. The graph on the left is obtained when forcing the discretized normal velocity to have average zero (as used throughout this paper). The graph on the right shows the volumes if one does not adjust the average of the normal velocity.

time $t$	$x$ -coordinate of the center	time $t$	$x$ -coordinate of the center
0	0.5878	25	0.9539
5	0.6328	30	0.9891
10	0.7099	40	1.005
15	0.8018	60	1.003
20	0.8893	80	0.9987

Fig. 4 Movement of the center of the asymmetrical dumbbell with a thick neck.

numerical scheme.

Also of interest is the movement of the center of gravity of the surface. The center moves right as the smaller bulge merges with the larger one, see Fig. 4. This effect is also quite visible in the graphs in Fig. 2.

## 4.2 A tube

In this numerical experiment we consider a cylindrical tube with spherical end-caps. The surface loses its convexity, however, the surface becomes convex again, and ultimately approaches a sphere. The experiment duplicates a results previously obtained in [11, 12]. For this experiment (see Fig. 5) the maximal edge-length was set to 1, the minimal edge-length to 0.1, and the time step to 0.01. The surface has 642 vertices and 1280 facets.

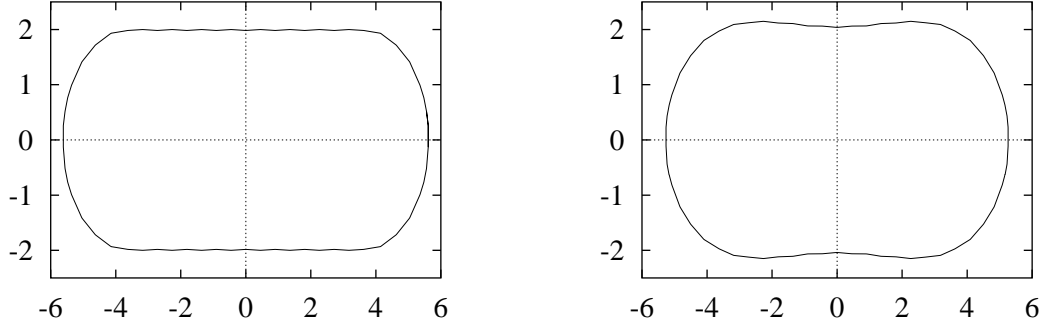


Fig. 5 These are cross-sections through a cylindrical tube. The left is the starting configuration, the right is at  $t = 3$ . Note that the second figure is not convex. The slight non-smoothness visible in the graphs stems from the triangulation, and can of course be reduced by taking more points. However, the point is that one can actually work with a rather coarse mesh and reduce computational cost, and still observe the occurring phenomena.

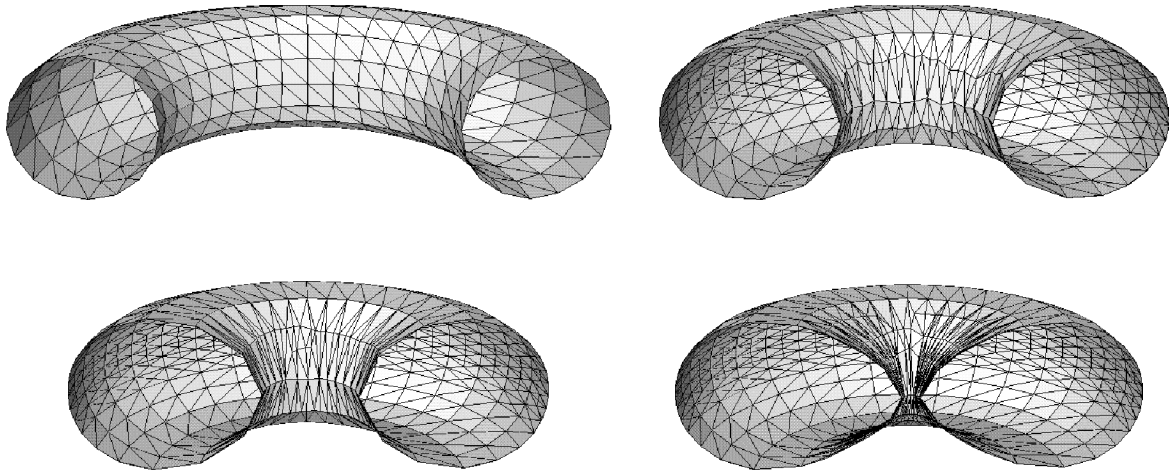


Fig. 6 A torus tightens the inner loop. The order of the snapshots of half of the torus is top left ( $t = 0$ ), top right ( $t = 3$ ), bottom left ( $t = 4$ ), bottom right ( $t = 4.251$ ). The main diameter of the initial torus is 8 units, while the minor diameter is 2 units.

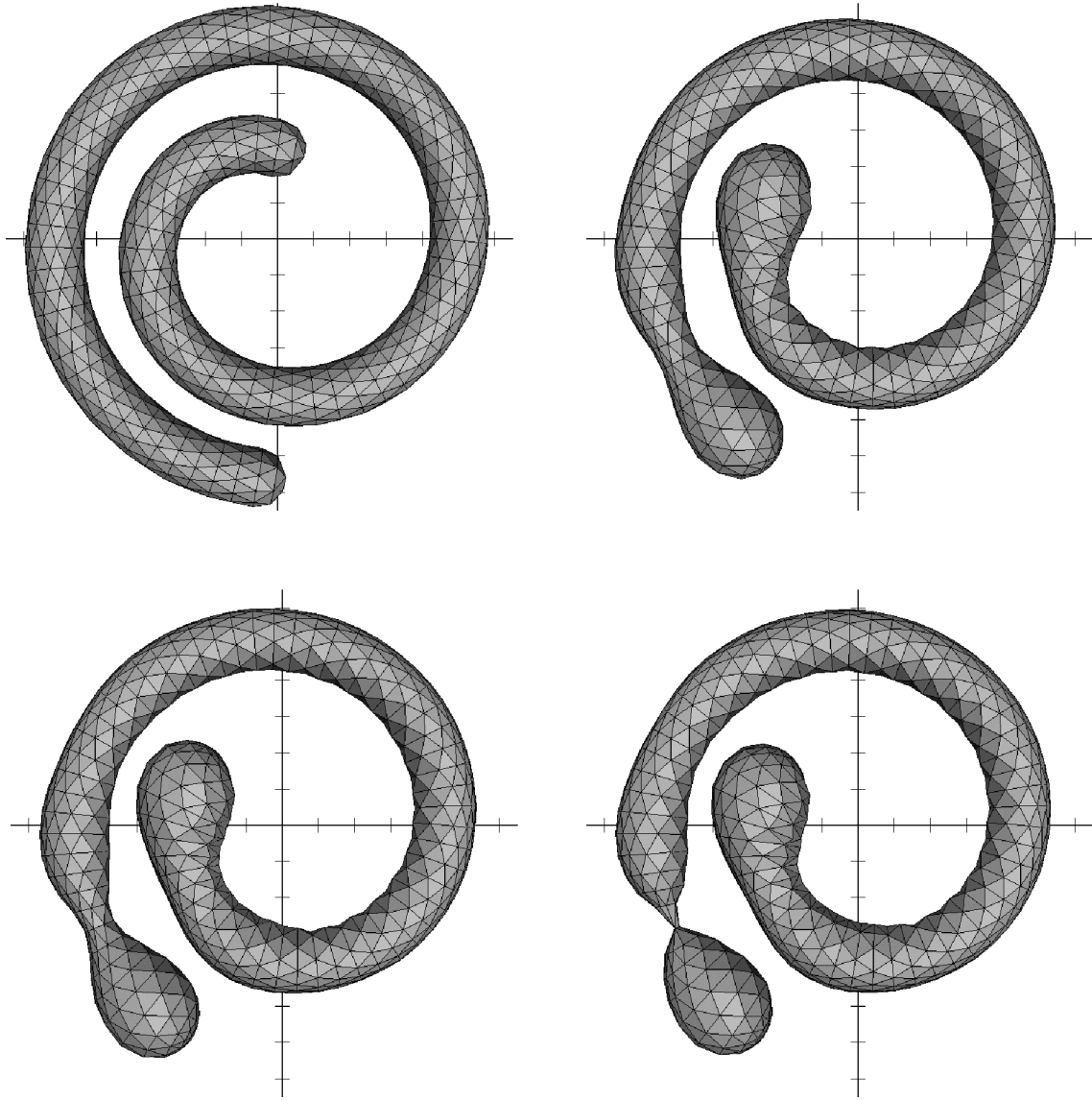


Fig. 7 A spiral develops a singularity. The order of the snapshots is top left ( $t = 0$ ), top right ( $t = 0.2$ ), bottom left ( $t = 0.25$ ), bottom right ( $t = 0.2709$ ). The tick marks on the axes are every 0.5 units.

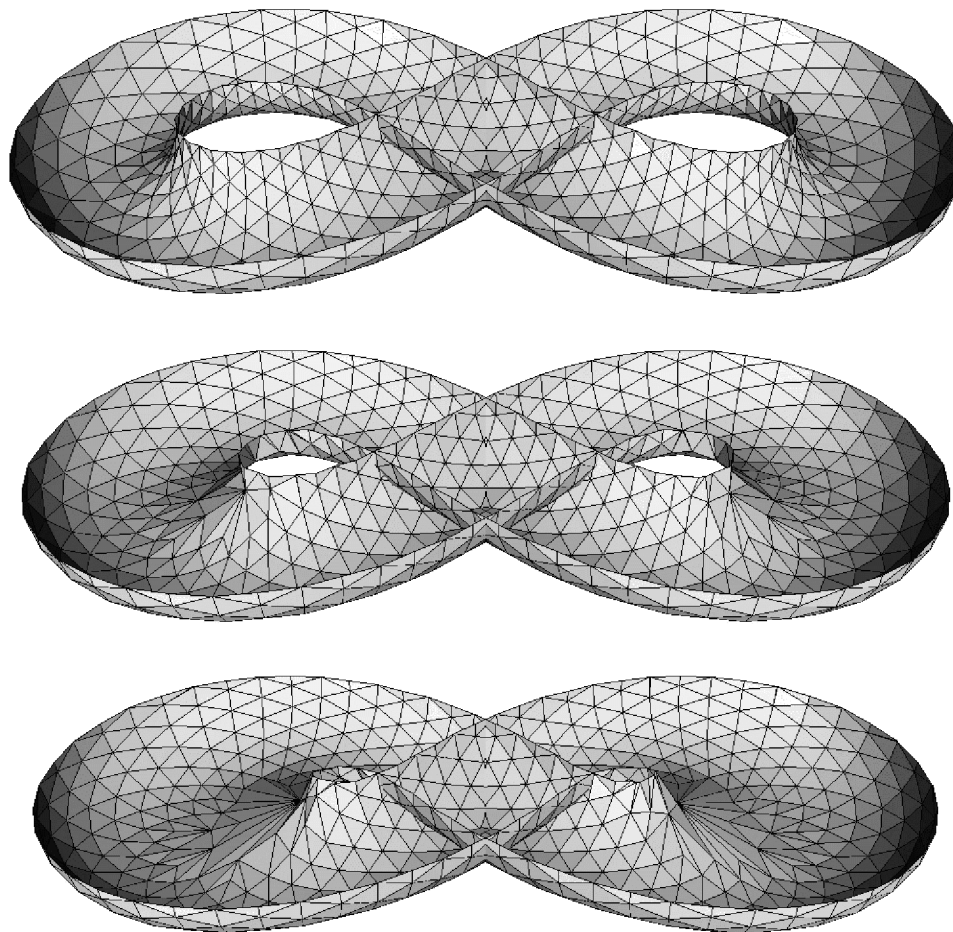


Fig. 8 The lower half of a tubular neighborhood of a figure eight. The order of the snapshots is top ( $t = 0$ ), middle ( $t = 0.02$ ), bottom ( $t = 0.035$ ). The extension of the surface is about 2.5 units in the  $x$ -direction, and about 1.2 units in the  $y$ -direction. The radius of the tubular neighborhood is about 0.2 units. Notice how the inner loops of the cross-section tighten.

### 4.3 A torus

The only embedded compact stationary surfaces for the surface diffusion flow are spheres, because spheres are the only embedded compact constant mean curvature surfaces [2]. Spheres are, of course, simply connected. Hence a torus must develop some interesting feature under this evolution, as it is not simply connected and can therefore not approach a sphere. The numerical experiment shows the torus tightens its loop about the central hole, and thus the curvature blows up. The evolution is remarkably similar to the one under the volume preserving (averaged) mean curvature flow (using the algorithm from [24], for example). For this experiment (see Fig. 6) the maximal edge-length was set to 0.75, the minimal edge-length to 0.01, the minimal thinness of facets to 0.005, and the time step to 0.001. The surface has initially 512 vertices and 1024 facets, and at the end of the experiment at  $t = 4.251$  the surface has 1235 vertices and 2470 facets. The changed number of vertices illustrates the adaptive scheme outlined in section 3.3.

### 4.4 A spiral

Here we investigate a tubular neighborhood of a spiral, the idea being to observe additional effects that are caused by bending a cylinder, and to exhibit the difference between two and three space dimensions. We have performed this experiment for various lengths of the spiral, and it seems that the surface always develops a singularity towards the less curved end, i.e. the outside end of the spiral. For a spiral in two space dimensions the reader is referred to [15]; there no singularity arises.

For this experiment (see Fig. 7) the maximal edge-length was set to 0.5, the minimal edge-length to 0.05, the minimal thinness of facets to 0 (which effectively disables thinness testing), and the time step to 0.0001. The surface has initially 978 vertices and 1952 facets, and at the end of the experiment at  $t = 0.2709$  the surface has 941 vertices and 1878 facets.

### 4.5 A figure eight

Here we investigate a tubular neighborhood of an (immersed) figure eight, to observe effects that are caused by the third space dimension. In two space dimensions a symmetrical figure eight contracts to a point in a fashion that seems almost self-similar [16], while in three space dimensions an essential singularity occurs.

For this experiment (see Fig. 8) the maximal edge-length was set to 0.4, the minimal edge-length to 0.05, the minimal thinness of facets to 0.01, and the time step to  $5 \cdot 10^{-6}$ . The surface has initially 1110 vertices and 2220 facets, and at the end of the experiment at  $t = 0.035$  the surface has 990 vertices and 1980 facets.

## References

- [1] D. ADALSTEINSSON AND J. A. SETHIAN, *A level set approach to a unified model for etching, decomposition, and lithography. III. Redecomposition, reemission, surface diffusion, and complex simulations*, J. Comput. Phys., 138 (1997), pp. 193–223.

- [2] A. ALEXANDROV, *Uniqueness theorems for surfaces in the large I*, Vestnik Leningrad Univ., 11 (1956), pp. 5–7.
- [3] N. D. ALIKAKOS, P. W. BATES, AND X. CHEN, *The convergence of solutions of the Cahn–Hilliard equation to the solution of the Hele–Shaw model*, Arch. Rational Mech. Anal., 128 (1994), pp. 165–205.
- [4] H. AMANN, *Linear and quasilinear parabolic problems. Vol. I*, Birkhäuser Verlag, Basel, 1995. Abstract linear theory.
- [5] P. BARAS, J. DUCHON, AND R. ROBERT, *Évolution d’une interface par diffusion de surface*, Comm. Partial Differential Equations, 9 (1984), pp. 313–335.
- [6] A. L. BERTOZZI, A. J. BERNOFF, AND T. P. WITELSKI, *Axisymmetric surface diffusion: Dynamics and stability of self-similar pinch-off*, J. Statist. Phys., 93 (1998), pp. 725–776.
- [7] J. BRADLEY, XV, 1053 Floyd Terrace, Bryn Mawr, Pennsylvania, USA, 1994.
- [8] J. W. CAHN, C. M. ELLIOTT, AND A. NOVICK-COHEN, *The Cahn–Hilliard equation with a concentration dependent mobility: motion by minus the Laplacian of the mean curvature*, Euro. Jnl. of Applied Mathematics, 7 (1996), pp. 287–301.
- [9] J. W. CAHN AND J. E. TAYLOR, *Linking anisotropic sharp and diffuse surface motion laws via gradient flows*, J. Stat. Phys., 77 (1994), pp. 183–197.
- [10] ———, *Surface motion by surface diffusion*, Acta metall. mater., 42 (1994), pp. 1045–1063.
- [11] B. D. COLEMAN, R. S. FALK, AND M. MOAKHER, *Stability of cylindrical bodies in the theory of surface diffusion.*, Physica D, 89 (1995), pp. 123–135.
- [12] ———, *Space-time finite element methods for surface diffusion with applications to the theory of the stability of cylinders.*, SIAM J. Sci. Comput., 17 (1996), pp. 1434–1448.
- [13] F. DAVÌ AND M. E. GURTIN, *On the motion of a phase interface by surface diffusion*, Z. Angew. Math. Phys., 41 (1990), pp. 782–811.
- [14] C. M. ELLIOTT AND H. GARCKE, *Existence results for geometric interface models for surface diffusion*, CMAIA Research Report, 94/22 (1994).
- [15] J. ESCHER, U. F. MAYER, AND G. SIMONETT, *On the surface diffusion flow*, in Proc. Intern. Conf. on Navier-Stokes Equations and Related Problems, TEV/VSP, Vilnius/Utrecht, 1997.
- [16] ———, *The surface diffusion flow for immersed hypersurfaces*, SIAM J. Math. Anal., 29 (1998), pp. 1419–1433.
- [17] P. C. FIFE, *Dynamical aspects of the Cahn–Hilliard equations*, Barret Lectures, University of Tennessee, (1991).

- [18] ———, *Seminar notes on curve shortening*, University of Utah, (1991).
- [19] M. GAGE AND R. S. HAMILTON, *The heat equation shrinking convex plane curves*, J. Differential Geom., 23 (1986), pp. 69–96.
- [20] Y. GIGA AND K. ITO, *On pinching of curves moved by surface diffusion.*, Comm. Appl. Anal., 2 (1998), pp. 393–405.
- [21] ———, *Loss of convexity of simple closed curves moved by surface diffusion.*, in Topics in nonlinear analysis. The Herbert Amann anniversary volume, J. Escher et al., ed., vol. 35 of Prog. Nonlinear Differ. Equ. Appl., Birkhäuser, Basel, 1999, pp. 305–320.
- [22] T. Y. HOU, *Numerical solutions to free boundary problems*, Acta numerica, (1995), pp. 335–415.
- [23] H. B. LAWSON, *Lectures on Minimal Submanifolds*, Publish or Perish, Berkeley, 1980.
- [24] U. F. MAYER, *A numerical scheme for moving boundary problems that are gradient flows for the area functional*, Europ. J. Appl. Math., 11 (2000), pp. 61–80.
- [25] U. F. MAYER AND G. SIMONETT, *Self-intersections for the surface diffusion and the volume preserving mean curvature flow*, Differential Integral Equations, (2000).
- [26] W. W. MULLINS, *Theory of thermal grooving*, J. Appl. Phys., 28 (1957), pp. 333–339.
- [27] T. MUNZNER, S. LEVY, AND M. PHILLIPS, *Geomview*, The Geometry Center, University of Minnesota, 1994.
- [28] R. L. PEGO, *Front migration in the nonlinear Cahn–Hilliard equation*, Proc. Roy. Soc. London Ser. A, 422 (1989), pp. 261–278.
- [29] A. POLDEN, *Curves and surfaces of least total curvature and forth-order flows*, Ph.D. dissertation, Universität Tübingen, Germany, (1996).
- [30] H. C. WENTE, *Counterexample to a conjecture of H. Hopf*, Pacific J. Math., 121 (1986), pp. 193–243.
- [31] ———, *Twisted tori of constant mean curvature in  $\mathbf{R}^3$* , in Seminar on new results in nonlinear partial differential equations (Bonn, 1984), Aspects of Mathematics, Vieweg, Braunschweig, 1987, pp. 1–36.

FB 17 Mathematik/Informatik  
 Universität Kassel  
 34109 Kassel, Germany  
 mayer@mathematik.uni-kassel.de